SOURCES, MECHANISMS AND CONTROL OF ROLL RESONANCE PHENOMENA FOR SOUNDING ROCKETS

by

D. A. Price, Jr.

Lockheed Missiles & Space Company
Sunnyvale, California

ABSTRACT

The results of a study to examine the dynamic flight characteristics of spin-stabilized sounding rockets during passage through the atmosphere is presented. Particular emphasis was placed upon the phenomena of roll resonance and the resulting motions leading to roll lock-in and catastrophic growth of the angle of attack. An understanding of the roll resonance phenomena and the sources and mechanisms leading to roll lock-in has been developed upon the basis of the steady state or equilibrium trim resonant response of spinning vehicles. The primary source of roll lock-in is shown to be the lateral center of gravity offset coupling with the aerodynamic normal force resulting from pitch resonant response to trim asymmetry. Induced roll moment degrades the roll resonant behavior instigated by c. g. -normal force coupling and is explained as a special case for mass and configuration asymmetries.

Realistic operational criteria are developed based on the equilibrium behavior yielding the worst possible combination of asymmetries for degradation of the roll control of the vehicle. The method allows definition, in a simple and precise manner, of the criteria and determination of asymmetry tolerances for avoiding roll lock-in while accounting for variations of vehicle and environment parameters.

Maximum tolerance limits for center of gravity and trim asymmetries (either aerodynamic trim or thrust misalignment) are specified for representative sounding rocket vehicles and trajectory profiles. The asymmetry tolerance limits were tested and verified numerically with a dynamic motion program. The effects of the time-varying environment show that the criteria based on equilibrium solutions yield conservative tolerances. Excellent agreement with flight behavior was obtained.

Methods for controlling roll rate during flight in the presence of configurational, mass. and thrust asymmetries are developed and a conceptual design for the most promising technique is illustrated.

NOMENCLATURE

A	Reference area and cross-sectional area of vehicle (ft^2)
b	$R\,(\bar{q}A/mV\omega)\left[C_{L_\alpha}(1-\nu)-\sigma(C_{m_q}+C_{n_{p\alpha}})\right]$
C_ℓ	Roll moment coefficient
C_{ℓ_δ}	Roll moment coefficient due to a differential fin cant, δ. on each fin
C_{ℓ_p}	Roll damping coefficient based on pd/2V
C_{m_α}	Pitch moment coefficient derivative
C_{m_q}	Pitch damping moment coefficient based on qd/V and referred to the center of gravity
C_{L_α}	Lift coefficient derivative
C_{N_α}	Normal force coefficient derivative
$C_{n_{p\alpha}}$	Magnus moment coefficient derivative
C_{ℓ_I}	Induced roll moment coefficient
C_A	Axial force coefficient
C_{m_o}	Moment coefficient representing an aerodynamic asymmetry
d	Reference length and diameter (ft)
I	Pitch moment of inertia (slug-ft^2)
I_x	Roll moment of inertia (slug-ft^2)
I_{sp}	Specific impulse (sec)
m	Mass (slugs)
p	Roll rate (deg/sec)
$\bar{q}$	Dynamic pressure (lb/ft^2)
r_e	Distance from center of gravity to nozzle throat (ft)
r_o	
T	Sustainer thrust as a function of time (lb)
V	Velocity (fps)
α	Angle of attack in body XZ plane (deg)
α_T	Total angle of attack (deg)
α_{ST}	Static trim angle of attack (deg)
α^*	Angle of attack for which C_{ℓ_I} changes sign
β	Angle of attack in body XY plane (deg)
Γ	Angle defining the orientation of the center of gravity offset (deg)
AGG	Center of gravity offset (in.)
Am	Center of gravity shift (in.)
δ	Fin cant angle (deg)
ϵ_T	Equivalent angular thrust misalignment, $Ra/12r_o$ (deg)
μ	Angle defining the orientation of the thrust misalignment (deg)
λ	Angle defining the orientation of the geometric asymmetry
θ	Arctan β/α
ψ	Phase angle, $h-\phi$ (deg)
ω	Natural frequency, $R\sqrt{-C_{m_\alpha}\bar{q}Ad/I}$, (deg/sec)

I. INTRODUCTION

Sounding rockets are usually developed with the requirements of low cost, high reliability, and flexible operation. One means of achieving low cost and flexible operation is to eliminate active guidance and control systems. The attainment of a high degree of reliability in placing the instrument payload into the desired environment requires good control over the sources of disturbances and minimization of the influence of these disturbances upon the subsequent vehicle dynamic motion behavior and trajectory dispersions. Sources of disturbances include such factors as deviations in launch attitude, mass and configurational asymmetries, thrust misalignment, atmospheric disturbances. and acroelastic bending. The effects of such disturbances upon the trajectory dispersion can he reduced hy providing the proper balance of aerodynamic and gyroscopic stability. However. inadequate control over the dynamic motion behavior can lead to unacceptable trajectory dispersions and possible

failure of the scientific experiment, or even result in structural failure.

As scientific experiments become more sophisticated and expensive, control of the launch vehicle performance and motion behavior assumes increased importance. In order to maintain the basic simplicity of sounding rockets, yet provide adequate motion control under a wide variety of experimental constraints, a better understanding was needed of the flight dynamic characteristics of the sounding rocket vehicle as a means to control the motion behavior.

Recent flight experience has exhibited varying degrees of motion disturbance during passage through roll resonance, i.e., where the spin rate is equal to the vehicle pitch frequency. Roll resonance of only momentary duration, as well as throughout the entire flight, has been observed. The accompanying pitch-yaw motion varied from only slight disturbances to rapid buildup of large angular motions with catastrophic results to the vehicle or experiment. Figure 1 illustrates motion behavior wherein roll resonance was maintained throughout the flight. The roll rate follows the decreasing aerodynamic pitch frequency rather than that programmed with differential fin cant. The angle of attack maintains a preferred orientation in the body and grows to large magnitude, yielding a flat spin after burnout. Furthermore, the observed behavior had not been predictable upon the basis of extant theory.

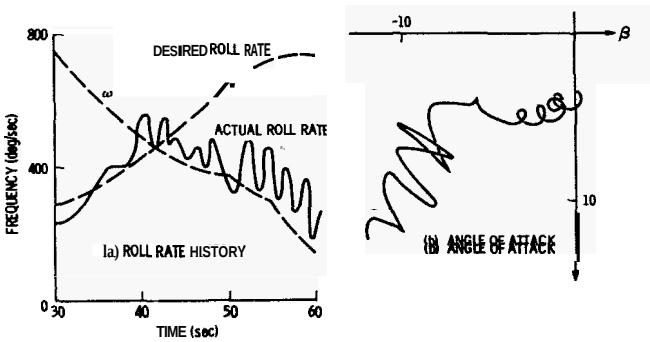

Fig. 1 Flight Behavior with Roll Lock-In

A considerable background of dynamic motion behavior theory is available for other applications such as ballistic reentry vehicles, air to air missiles. and aerodynamic test rockets[1-8]. Most of these theories were limited to conditions of constant vehicle inertial parameter, trajectory environment, and aerodynamic characteristics. or for a time-varying environment with fixed vehicle characteristics and spin. Glover7 studied roll rate changes resulting from mass and configurational asymmetries for a symmetrical reentry body with time-varying environment by means of 6-D digital simulation.

For sounding rockets, all of these vehicle and environment characteristics are variable, including thrust application, and tend to complicate the problem significantly. The influence of thrust misalignment and induced roll moment was studied briefly by means of 6-D digital simulation[9]. Herbert and Merchant[10] developed a steady state theory for roll lock-in from induced roll moment effects and pitch trim response in the vicinity of roll resonance for sounding rockets. Static stability of roll response was shown for the steady state theory and demonstrated for varying environments with 6-D digital simulation. The latter two studies for sounding rockets were able to demonstrate roll lock-in phenomena but required inordinately large magnitudes of induced roll moment and thrust asymmetry. Glover's results also indicated configurational asymmetries larger than expected from current operational experience for reentry vehicles.

Technical Approach

The primary emphasis was placed on dynamic motion response at small angles of attack. The philosophy here is that understanding of the pitch-yaw and roll response at very small angles of attack will lead to capability to control the flight dynamic response and forestall roll lock-in and catastrophic growth of yaw. Furthermore, it was found that the roll lock-in phenomena can be explained and demonstrated on the basis of small angle motion and linear aerodynamics in pitch. Consideration of nonlinear aerodynamic characteristics in roll (e.g., induced roll moment) appeared necessary, even at small angles of attack,

The results of the work performed during the study are presented in the subsequent sections. The basic understanding of roll lock-in behavior is developed in Section11 by means of a "phenomenological" approach to the sources and mechanisms of roll resonance. Section III derives the operational criteria and asymmetry tolerances for forestalling the operational roll lock-in and demonstrates the numerical verification of the operational criteria. Section IV develops in-flight motion control techniques and describes a promising conceptual design.

11. ROLL RESONANCE PHENOMENA

Perhaps the most fundamental assumption propounded herein is that the roll resonance phenomena can be explained by, and roll lock-in criteria can be defined upon, the basis of the steady state or equilibrium trim resonant response of a spinning vehicle, It is not obvious "a priori" that this assumption will apply to a sounding rocket such as the Aerobee 150A in view of varying environment, spin rate, and aerodynamic characteristics. This section will demonstrate that excellent insight into the mechanism of roll lock-in and the subsequent motion behavior is gained by consideration of the equilibrium or steady state trim conditions. The general Characteristics of the motion behavior will, of course, be altered to some extent by the time-varying environment, Nevertheless, the essence of the roll control problem for a slowly changing environment, such as encountered by the Aerobee 150A vehicle, is revealed by the character of the equilibrium solution.

Definition of Roll Lock-In

The previously accepted terminology for "roll lock-in" was somewhat ambiguous in terms of duration and magnitude of roll disturbance and subsequent pitch-yaw motion control. For example. if the spin rate were nearly equal to the pitch natural frequency for any length of time, however short, the vehicle was considered "locked-in." The duration of this locked-in condition profoundly affects the ability to recover the nominal roll rate and reduce angle of attack deviations to acceptable values.

Therefore, to clarify the analyses and discussions to follow, a particular and restricted definition of roll lock-in is adopted. The term "roll resonance" is applied to the condition where the roll rate is maintained nearly equal to the natural aerodynamic frequency. "Roll lock-in" is construed to mean forced "roll resonance'! throughout the atmospheric portion of flight

Sources of Disturbances

The inevitable geometrical. inertial, and operational asymmetries resulting from manufacturing and assembly tolerances. fin adjustment, measurement inaccuracies, and random flight environment uncertainties provide the genesis for the loss of roll control and subsequent undesirable pitch-yaw motion behavior, Such asymmetries can be classified conveniently into three principal categories: configurational, mass distribution, and aerodynamic-geometrical interactions. Configurational asymmetries

cause an effective change in fin cant and/or a static trim angle of attack through an aerodynamic moment or thrust moment. Mass distribution deviations cause a change in the static stability margin and static trim angle of attack, rotation of the axes of the principal moments of inertia, and provide roll coupling with the aerodynamic normal force, Aerodynamic-geometrical interactions cause phenomena such as the well known induced roll moment for finned or winged bodies and aeroelastic bending.

These asymmetries were characterized in terms of an effective aerodynamic trim asymmetry (C_{m_0}), an effective thrust misalignment angle (ϵ), and the effective center of gravity lateral offset (ACG). While these quantities may be difficult to measure directly for a given vehicle, they provide simple and useful parameters for developing a mathematical model of the roll resonance phenomena. Furthermore, since these parameters are treated as "effective" asymmetries, the qualitative effects of more complex sources (such as aeroelastic bending, for example) can be deduced from the results for the simpler concept developed in this analysis.

Motion Behavior With No Mass Asymmetry

Nelson[2] developed the equations of motion and their solutions in the body fixed axis system (depicted in Fig. 2) for a symmetric spinning vehicle with small longitudinal asymmetries. The resulting complex angle of attack $\zeta = \beta + i\alpha$ is described in Fig. 3 by two time-varying damped vectors, R_1 and R_2, rotating at different rates, $\omega_o - A\omega$ and $\omega_o + A\omega$, respectively, about the trim component α_{TRIM}. The term ω_o represents the damped natural frequency of the system, whereas the $A\omega$ quantity is essentially the gyroscopic spin frequency. Note that for positive spin rate p, the R_2 vector always rotates faster than R_1 in a counterclockwise direction. The R_1 vector changes its direction of rotation, depending on the relative magnitude of ω_o and $A\omega$. The α_{TRIM} position varies primarily with the proximity to resonance (i.e., $\omega_o = A\omega$) and its magnitude with the environment.

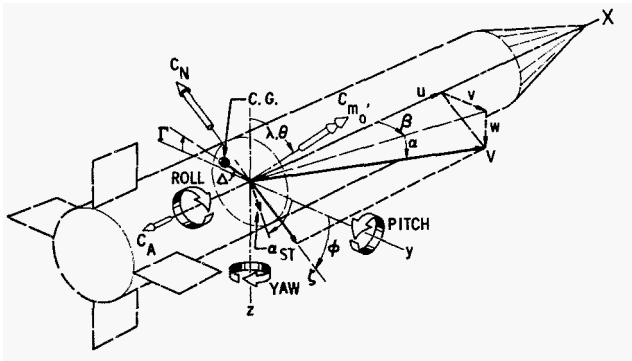

Fig. 2 Axis System and Nomenclature

Typical motions are illustrated in Fig. 4 for a constant environment with spin rates below, at, and above resonance. When below resonance, the R_1 vector rotates clockwise about the trim to yield the familiar pattern with outside loops. Above resonance, the counterclockwise motion of R_1 yields an inside loop pattern, while at resonance R_2 it describes a circle around the stationary R_1. Note that the trim component α_{TRIM} orientation changes only with proximity to resonance.

With a c.g. displaced from the geometric (or aerodynamic) centerline, a roll torque is generated by the resultant normal force, whose magnitude and direction depends on the magnitude and orientation of the total angle of attack ζ. Since the R_1 and R_2 vectors prescribe motions about the trim component, the average

$$\ddot{\beta} + A_1\dot{\beta} - A_2\dot{\alpha} - B_1\beta + B_2\alpha = C_1$$

$$\ddot{\alpha} + A_1\dot{\alpha} + A_2\dot{\beta} - B_1\alpha - B_2\beta = C_2$$

$$A_1 = \frac{\bar{q}A}{m\bar{V}}\left(C_{L_\alpha} - \frac{md^2}{I}C_{m_q}\right) + \frac{T}{m\bar{V}} + \frac{Tr_o^2}{I_g I_{sp}}$$

$$A_2 = p(2 - I_x/I)$$

$$B_1 = C_{m_\alpha}\bar{q}Ad/I + p^2(1 - I_x/I)$$

$$B_2 = -p\frac{\bar{q}A}{m\bar{V}}\left[C_{L_\alpha}\left(1 - \frac{I_x}{I}\right) - \frac{md^2}{I}\left(C_{m_q} + C_{n_{p_\alpha}}\right)\right]$$

$$-p\frac{T}{m\bar{V}}\left(1 - \frac{I_x}{I}\right) - p\frac{Tr_o^2}{I_g I_{sp}} - \dot{p}$$

$$C_1 = \left(C_{m_o}\cos\lambda - C_A\frac{\Delta CG}{d}\cos\Gamma\right)\frac{\bar{q}Ad}{I} + \frac{Tr_e\epsilon}{I}\cos\mu$$

$$C_2 = \left(C_{m_o}\sin\lambda - C_A\frac{\Delta CG}{d}\sin\Gamma\right)\frac{\bar{q}Ad}{I} + \frac{Tr_e\epsilon}{I}\sin\mu$$

SOLUTIONS

$$\zeta = \alpha_{TRIM} + R_1 e^{i\nu_1} e^{\left[\lambda_o + \Delta\lambda + i(\omega_o - \Delta\omega)t\right]} + R_2 e^{i\nu_2} e^{\left[\lambda_o - \Delta\lambda - i(\omega_o + \Delta\omega)t\right]}$$

$$\alpha_{TRIM} = -C/B$$

Fig. 3 Equations of Motion

roll torque is seen to be generated by the trim angle of attack α_{TRIM}. Hence, in the subsequent development, only the trim component will be considered. This is equivalent to assuming that the dynamic components R_1 and R_2 have damped to negligible magnitudes or that steady-state equilibrium trim conditions exist.

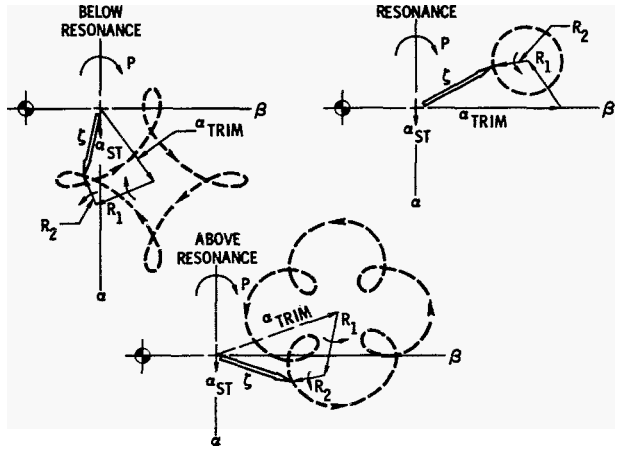

Fig. 4 Total Angle of Attack Motions

Trim Resonant Response Characteristics

Typical rolling trim response of the spinning vehicle to static longitudinal trim asymmetry is presented in Fig. 5 in terms of the spin rate to aerodynamic pitch frequency ratio p/ω. When the characteristic forcing frequency w approaches the gyroscopic precessional frequency $p\sqrt{1 - I_x/I}$, the familiar amplification of the static deflection α_{ST} and a phase shift ψ occur. This response is shown schematically in Fig. 5 for representative trajectory conditions at several altitudes (i.e., constant w).

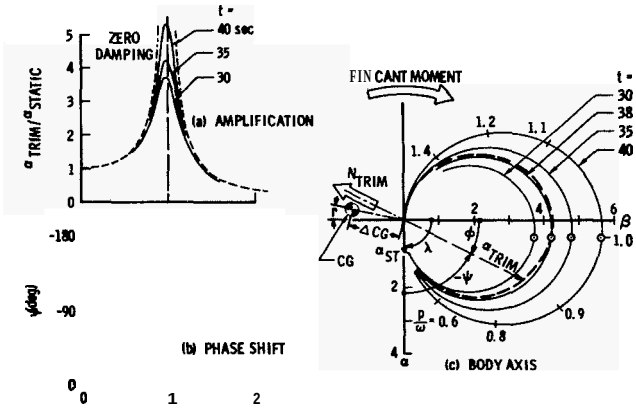

Fig. 5 Rolling Trim Response

Figure 5a depicts the large magnification of the zero spin static trim α_{ST} as spin rate approaches resonance ($p/\omega \approx 1$) with subsequent decay toward zero for large p/ω. The peak magnification depends upon the effective aerodynamic damping for the vehicle and trajectory conditions under consideration. Note that large amplitudes are reached only in close proximity to resonance. For sounding rockets such as the Aerobee 150A, the peak occurs virtually at $p = \omega$.

The relative orientation of the trim angle of attack with respect to the static trim undergoes a radical phase shift during passage through resonance, as depicted in Fig. 5b. At resonance, a phase shift ψ close to –90 deg occurs and approaches –180 deg for large p/ω. This phase change is seen to undergo a large change in close proximity to resonance while the amplification changes little. Hence, large trim angles of attack are maintained over a phase shift on the order of ±45 deg about resonance.

These characteristics of the trim response are illustrated more clearly in Fig. 5c in terms of the complex angle of attack components α and β. With increasing p/ω the static trim α_{ST} rotates counterclockwise and grows to the peak magnitude with $\psi \approx -90$ deg at resonance ($p/\omega \approx 1$). A further increase of p/ω above resonance rotates and decreases the trim angle of attack toward $\alpha_{TRIM} = 0$ and $\psi = -180$ deg. Since the longitudinal asymmetry is fixed within the body, this whole pattern rotates with the body at spin rate.

The equilibrium trim response for a varying environment and spin rate (with no roll disturbances) would then follow the heavy dashed curve superimposed on Fig. 5. Because of the high pitch and roll damping inherent for current sounding rocket design, the dynamic motions follow the equilibrium resonant response quite closely, as illustrated in Fig. 6. The actual roll rate is identical to the steady state value at nominal resonance (32 sec) and lags by only 2 percent at 40 sec, increasing to a maximum 27 percent at burnout. While the peak amplification of the angle of attack is significantly reduced at resonance, the character of the equilibrium trim response with changing p/ω is clearly evident. The initial growth

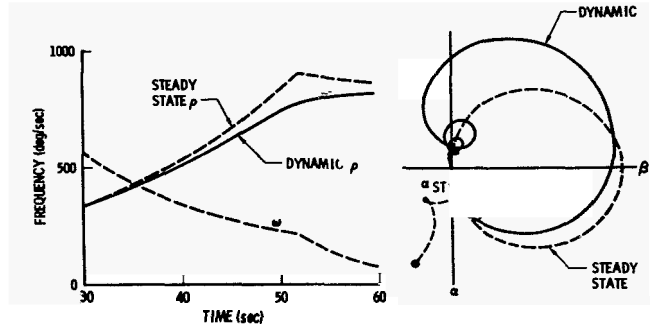

Fig. 6 Response With Variable Environment

of the angle of attack lags behind the equilibrium trim primarily due to the pitch inertia. After the peak trim is passed, the driving force (i.e., out-of-trim) is reduced until the dynamic angle of attack exceeds the current trim with subsequent oscillation about trim quickly damping out. Initial out-of-trim motions also damp quickly.

If proximity to resonance is extended, the dynamic response will approach the equilibrium trim more closely because there is a longer time to respond to the out-of-trim condition. Hence, the disturbances which cause roll resonance essentially suppress the dynamic motion response and yield equilibrium conditions. Therefore, the assumption of equilibrium trim resonant response for the spinning vehicle appears eminently justified,

Mechanism of Roll Resonance

The coupling between the pitch and roll mode is illustrated in Fig. 5c for the pitch resonant trim. The normal trim force N_{TRIM}, caused by the pitch trim angle of attack α_{TRIM}, yields a spin-down moment about the c.g. opposing the fin cant moment. As spin rate and pitch frequency vary, the asymmetry roll moment can change direction. For example, if ψ were greater than A, the c.g. –normal force coupling would yield a spin-up moment. When the normal force is aligned with the c.g., the roll moment degradation is zero.

$$I_x \dot{p} = T\epsilon a + \bar{q}Ad\left\{\delta C_{\ell_\delta} + C_{\ell_p}\frac{pd}{2V} - C_{\ell_I}\sin N\phi - \frac{\Delta CG}{d}C_{N_\alpha}\alpha_{TRIM}\sin(\phi - \Gamma)\right\}$$

where

$$\alpha_{TRIM} = \frac{\alpha_{STATIC}}{\sqrt{\left[1 - \frac{p^2}{\omega^2}\left(1 - \frac{I_x}{I}\right)\right]^2 + \left(\frac{bp}{\omega}\right)^2}}$$

$$\tan\psi = \frac{\frac{bp}{\omega}}{1 - \frac{p^2}{\omega^2}\left(1 - \frac{I_x}{I}\right)}$$

$$\omega = \sqrt{\frac{-C_{m_\alpha}\bar{q}Ad}{I}}$$

$$b = \frac{\bar{q}A}{mV\omega}\left[C_{N_\alpha}\left(1 - \frac{I_x}{I}\right) - \frac{md^2}{I}Cmq\right]$$

$$\vartheta = \lambda - \psi$$

Fig. 7 Available Roll Torque Equation

The available roll acceleration from the fin cant, $\delta C_{\ell_\delta} + C_{\ell_p}\frac{pd}{2V}$, the c.g. –normal force coupling $\Delta CG\, C_{N_\alpha}\alpha_{TRIM}\sin(\phi - \Gamma)$. induced roll moment $C_{\ell_I}\sin N\phi$, and thrust misalignment and offset $T\epsilon a$ for this arrangement of asymmetries is shown in Fig. 7. Note that the magnitude of the trim angle of attack depends primarily upon the proximity of resonance p/ω while the orientation ϕ varies with the effective aerodynamic

damping as well. The direction and magnitude of the roll acceleration due to the asymmetry coupling clearly depends upon the relative orientation ($\phi - \Gamma$) of the c.g. offset and aerodynamic trim asymmetry. The induced roll contribution depends on the magnitude and absolute orientation ϕ of the trim angle of attack only. All of the quantities entering into the roll equation can be specified throughout the trajectory. When the magnitude of the asymmetry terms cancel the fin cant terms, a roll trim ($\dot{p} = 0$) will occur. The roll trim soiutions will be developed graphically in order to illustrate the mechanisms of roll resonance more clearly.

Roll Trim for C.G.-Normal Force Coupling ($C_{\ell_I} = 0$)

The coupling is presented in Fig. 8 for an axis system through the c.g. and with the particular arrangement of the asymmetries shown in Fig. 8a. This relative orientation yields the maximum increase in roll moment below resonance.

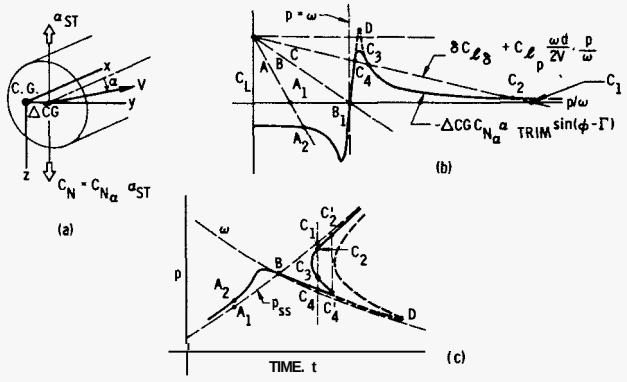

Fig. 8 Roll Resonance with C.G. Offset

In Fig. 8b, the variation of the aerodynamic roll moment coefficient with p/ω is illustrated in terms of the negative of the c.g.-normal force coupling [$-\Delta CG\ C_{N_\alpha}\ \alpha_{TRIM} \sin(\phi - \Gamma)$] and the fin cant contribution $\delta C_{\ell_\delta} + C_{\ell_p}\, wd/2V\ (p/\omega)$. For a given time in the trajectory, the fin cant term yields an inclined straight line intersecting the abscissa at the ideal steady state spin rate (e.g., point A_1). The amplification and orientation change of the resonant trim angle of attack with respect to the c.g. offset yields the rapid change in the asymmetry coupling term in the vicinity of resonance. The intersections (e.g., A_2) of the curves then represent possible roll trim conditions.

The variation of these roll trim solutions can be easily traced for a slowly changing environment by examining the effect of ω and V on the shape of the curves in Fig. 8b. The primary change occurs in the slope of the $C_{\ell_\delta}\ \delta + C_{\ell_p}\ \omega d/2V(p/\omega)$ lines labeled A. B and C. The change of the ACG $C_{N_\alpha}\ \alpha_{TRIM} \sin(\phi - \Gamma)$ contour is much smaller (omitted here for the sake of clarity) and effects mainly the magnitude of the peak as was noted in Fig. 5. Early in the flight. where ω/V is large, only one equilibrium solution (A_2) exists for p slightly larger than for the ideal value (A_1). With increasing time (decreasing ω/V) the solution moves to B_1 and is equivalent to the ideal value. With further decrease in ω/V, the equilibrium spin rate closely follows the natural frequency ω .i.e., roll resonance. Multiple solutions appear also as depicted by line C for which points C_2 and C_4 represent stable solutions and point C_3 is unstable. It is immediately evident that solution C_4 is retarded with respect to the ideal point C_1 by a significant amount until the peak of the $\Delta CG\ C_{N_\alpha}\ \alpha_{TRIM} \sin(\phi - \Gamma)$ curve is attained (i.e., C_3 and C_4 merge). Since point C_3 is unstable the roll rate will "jump" to a point corresponding to C_2. Note that the solutions typified by C_4 are always in the vicinity of resonance (i.e., $p/\omega \cong 1$) due to the character of the angle of attack resonance response. Hence, the period of time for passage through roll resonance is significantly extended by the c.g.-normal force roll coupling and presages the buildup of large angle of attack disturbances. Now, if the peak of the ACG $C_{N_\alpha}\ \alpha_{TRIM} \sin(\phi - \Gamma)$ contour is sufficiently high, roll "lock-in" is assured. This is depicted in Fig. 8b where the ($C_{\ell_\delta}\ \delta + C_{\ell_p}\ pd/2V$) curve passes through or below point D with zero slope (corresponds to infinite time or zero ω). For this situation the roll rate cannot escape from the near resonance conditions and thus will remain locked-in. In addition, the peak magnitude D increases with decreasing ω thus further aggravating the lock-in condition.

The corresponding variation of the roll rate with respect to the ideal steady state rate is illustrated in Fig. 8c. The typical solutions A, B and C from Fig. 8b are depicted to illustrate the correlation with the roll moment diagram. The roll rate lead at low ideal roll rates A is clearly evident. Crossover to a lag occurs at B until the three solutions of C are reached.

The stable solution C_4 remains close to the natural aerodynamic frequency for an extended period of time. As seen in Fig. 8b, this "tongue" results from the peak amplitude of the angle of attack. The tip C_4' corresponds to the merger of points C_3 and C_4. For steadily increasing time, a jump must occur from C_4' to C_2' near the ideal roll rate. If, however, the tip of the tongue stretches to a time where the vehicle is essentially out of the atmosphere, illustrated by point D, a condition of roll lock-in exists. This restricted definition of roll lock-in was adopted for this study.

The c.g.-normal force coupling behavior discussed thus far is for a particular orientation of the asymmetries. The other extreme is found where the c.g. offset and static trim angle of attack lie in the same plane. For this arrangement, the initial roll disturbance is zero but will reach higher magnitudes near roll resonance due to the trim angle of attack phase change. Although the roll moment disturbance appears in one direction only, equilibrium solutions similar to condition C in Fig. 8c occur in the vicinity of resonance. Hence. c.g. and configurational asymmetries of a random nature can lead to roll resonance phenomena and possible lock-in.

Typical equilibrium solutions of the roll equation of Fig. 7 obtained with the aid of the digital computer are illustrated in Fig. 9 for a C_{m_o} of 1.0. This magnitude of the trim asymmetry corresponds to a static trim angle of attack of about 1.5 deg at burnout for the Aerobee 150A. Figure Sa, with $\lambda = 270$ deg, corresponds to the case developed schematically in Fig. 8. As expected, the roots tend to fall near either the steady state roll rate,

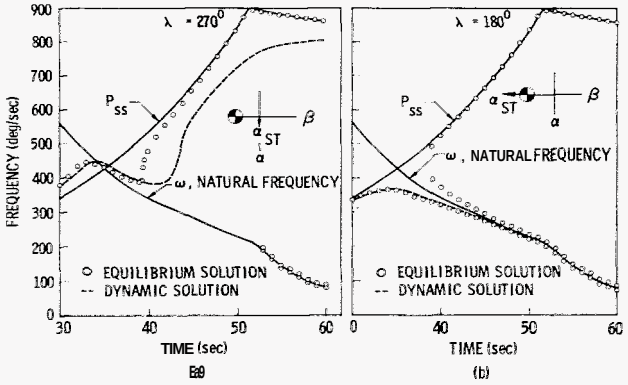

Fig. 9 Roll Resonance Solutions Neglecting Induced Roll Moment ($\Delta CG = 0.1$ In.)

p_{ss}, or the natural. frequency, w corresponding to roll resonance. The roots corresponding to C_3 and C_4 merge and disappear after 40 sec. These roots reappear later (53–60 sec) due to the very large trim amplification at high altitude. This "gap" in the existence of roots near the natural frequency is desirable since this allows a vehicle to break out of roll resonance (the "jump" from C_4' to C_2') and thus avoid catastrophic yaw and increase the roll rate past any unstable roots which may occur later. Figure 9b illustrates that roll lock-in, and thus catastrophic yaw, can be expected for A = 180 deg since roots near w exist throughout the entire trajectory. The utility of the equilibrium solution for predicting the roll behavior is demonstrated by the dynamic solutions shown in Fig. 9.

The dynamic solution for λ = 270 deg demonstrates the breakout from roll resonance when a gap in the roots exists. The dynamic solutions for λ = 180 deg maintains roll resonance until the angle of attack limit is exceeded. The initial conditions were chosen *so* that the vehicle is initially trimmed (i.e., in equilibrium). Except, then. for a lag due to the changing environment and inertia of the vehicle, the dynamic solution follows and thus substantiates the analysis of the equilibrium solutions.

Lateral C. G. –Trim Asymmetry Coupling With Induced Roll Moments

The induced roll moments act in a manner similar to the roll coupling from c. g. offset and trim angle of attack resonant response with the additional complication of the relative orientation of the fins and the angle of attack plane. This coupling is illustrated in Fig. 10. A typical variation of induced roll moment C_ℓ with total angle of attack is shown in Fig. 10a[11]. The data is seen to be

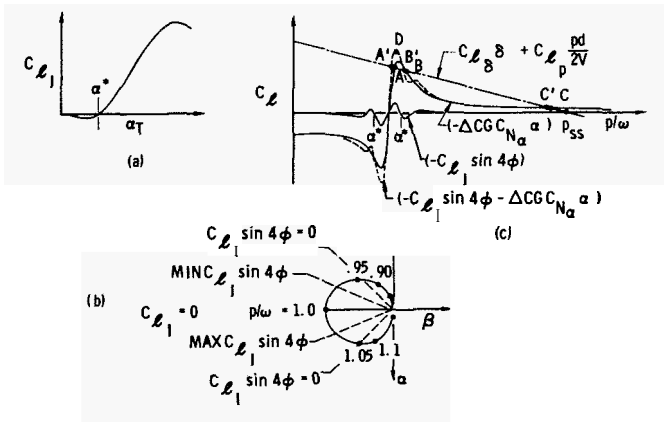

Fig. 10 Induced Roll Moment Effect

negative at small angles, and reversing to positive values for angles of attack greater than α^*. The corresponding angles of attack α and sideslip β are shown in Fig. 10b to illustrate the orientation within the body. Note that due to the rapid change of the phase angle ϕ with spin rate in the vicinity of resonance, the total angle of attack sweeps through four regions of maximuminduced roll moment for tho Aerobee 150A vehicle (according to the sin 4 ϕ formulation).

These induced roll moment characteristics alter the variation of the rolling moment coefficient with p/ω, as shown in Fig. 10. Note that multiple solutions can occur for the induced roll moment alone due to the phase orientation and sign reversal of C_{ℓ_I} for α^*. However, for small angles of attack, the magnitudes of the C_{ℓ_I} sin 4 ϕ term are usually small compared to the $\Delta CG\, C_N$ term[11] and can be expected to introduce only a small roll rate disturbance during passage through resonance. But, when added to the c.g.–trim coupling term, the induced roll moment can increase the peak magnitude (point D) sufficiently to extend the roll resonance duration significantly.

It is evident from these considerations that the mechanism and character of the roll resonance phenomena with induced roll moments is essentially that obtained with c.g. offset in the presence of pitch trim asymmetry. Furthermore, at small angles of attack, the induced roll moment serves primarily to extend the roll resonance resulting from c.g. and/or thrust asymmetry coupling with trim asymmetry rather than to instigate the resonance.

Roll lock–in with induced roll moments thus represents a special case for lateral c.g.–normal force coupling phenomena. When the c.g. offset is zero (a highly unlikely event), a large angle of attack is required to cause sufficient induced roll moment. This. in turn, requires a large aerodynamic trim asymmetry or thrust misalignment. This situation is illustrated in Fig. 11 for dynamic solution with ACG = 0. A large magnitude of the aerodynamic trim asymmetry (C_{m_0} = 0.75) is necessary to cause roll lock–in. The underlying reason is shown in Fig. 11b where the angle of attack for the smaller C_{m_0} never exceeds α^* degrees, for which the induced roll moment remains small.

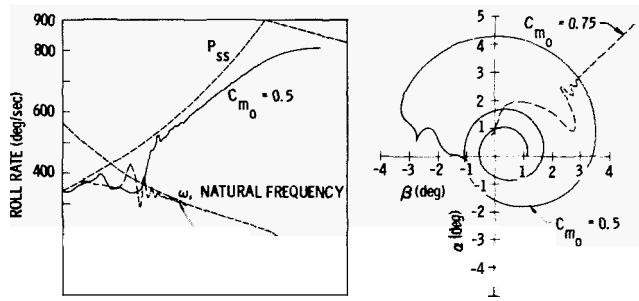

Except for somewhat higher roll rate fluctuations, these results are similar to those depicting c.g. effects, i.e., a roll resonance condition for the larger asymmetry with subsequent catastrophic yaw. and a temporary roll resonance condition with the reduced asymmetry and subsequent recovery of the angle of attack and roll rate.

III. DEVELOPMENT OF OPERATIONAL CRITERIA

Utilization of the equilibrium trim response characteristics allows definition of realistic operational criteria and determination of tolerance limits for the asymmetries in a particularly simple and precise manner without the need for successive trials with a digital computer. This section presents the philosophy and technique for determination of these tolerances, including the implications of operational requirements.

Worst Condition Philosophy

The asymmetries considered in this study are. by nature, random in magnitude and orientation. Therefore, analysis of the influence of the random arrangement of such asymmetries becomes time consuming and requires interpretation upon the basis of probability of occurrence. A more direct approach is to select the arrangement of the asymmetries yielding the greatest degradation of the roll moment, and to evaluate the minimum magnitude of each asymmetry which will cause roll lock–in. Any other

relative orientation of the asymmetries will have a smaller effect on roll moment for this minimum magnitude and, therefore, will not cause roll lock-in, although roll resonance may occur temporarily.

The equilibrium analysis technique allows an exact definition of the worst conditions, as illustrated in Fig. 12, for a c.g. offset ACG and an aerodynamic trim asymmetry C_{m_0} and/or a thrust misalignment ε. Assuming the fin cant has been set to provide a positive roll rate, the relative orientation of the normal force C_N resulting from the peak resonant angle of attack α_T and the lateral c.g. offset is selected to cause maximum negative roll acceleration. This orthogonal arrangement is then oriented with respect to the fins to yield the maximum effect from the induced roll moment characteristics. For angles of attack greater than α^* (see Fig. 10a), the direction of the roll acceleration due to the induced roll moment term alternates, as shown in Fig. 12a by plus and minus signs, The maximum magnitude

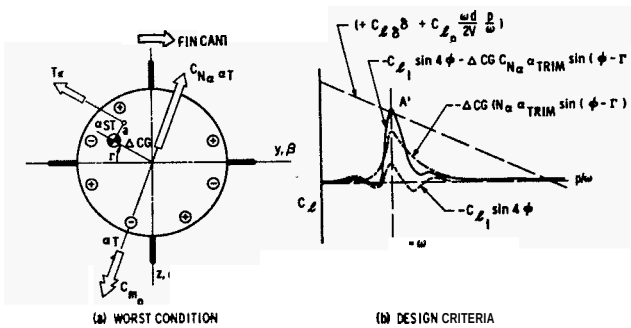

Fig. 12 Definition of Design Criteria

occurs at orientation angles of 22 1/2 ± n 90 deg, according to the sin 4 @ approximation. (Wind tunnel results can be used in a similar manner to select more exactly the "worst" orientation for a particular angle of attack.) An orientation of Γ = 22-1/2 deg is illustrated in Fig. 12a.

For the assumption of equilibrium trim response, the static trim angle of attack, α_{ST}, would be essentially colinear with ACG. The variation of the rolling moment coefficient with p/ω for this "worst condition" arrangement of asymmetries is illustrated in Fig. 12b. At a particular time in the trajectory, the minimum magnitude of the asymmetries causing roll resonance is indicated by point A'. The situation depicted by point A' then represents the criterion for roll lock-in. Any other orientation of the asymmetries will yield a magnitude of the roll coupling lower than that of point A' and hence will breakout from roll resonance at that particular time in the trajectory.

Determination of Tolerances

With this criterion, the equations of motion of Fig. 3 reduce to the specification of the c.g. offset required to maintain roll resonance throughout the flight, namely:

$$ACG = \frac{d}{\alpha_T C_{N_\alpha}} \left(\delta C_{\ell_\delta} + C_{\ell_p} \frac{\omega d}{2V} - C_{\ell_I} \sin 4\Gamma \right)$$

where

$$\left.\begin{aligned} \alpha_T &= \frac{\alpha_{ST}}{b} \\ p/\omega &= 1 \\ \psi &= \pi/2 \end{aligned}\right\} \quad \frac{I_x}{I} << 1, \quad b << 1$$

Since all of the quantities are known along the trajectory, a straightforward calculation of the ACG required *to* maintain p ≈ w can be made for a given trim asymmetry (C_{m_0} or ε_T) and orientation (Γ). The only assumptions included are equilibrium trim response, linear aerodynamics (except for C_{ℓ_I}), and small angles. Time-varying coefficients can be accounted for.

Typical ACG histories for C_{m_0} are presented in Fig. 13 for the range of Γ encompassing the maximum and minimum magnitudes of the induced roll term. The

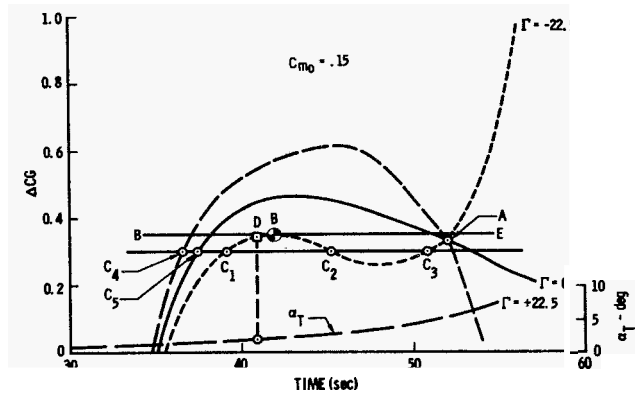

Fig. 13 ACG Required for Resonance

three curves then represent the envelope of all possible values of the ACG required for roll resonance between Γ = ±22.5 deg. At nominal resonance (35 sec), no lateral c.g. offset is needed, since the fin cant and damping are in balance at p = w. After nominal resonance, the fin damping term $C_{\ell_p}(\omega d/2V)$ decreases with w and increasing ACG is required to account for the difference between fin cant and damping. As the resonant trim angle of attack grows with time, the normal force increases more rapidly than the difference between δC_{ℓ_δ} and $C_{\ell_p}\omega d/2V$, resulting in a smaller ACG required for maintaining roll resonance. Prior to nominal resonance, a negative ACG (or 180 deg orientation shift) is needed since the fin damping $C_{\ell_p}\omega d/2V$ is larger than the fin cant δC_{ℓ_δ}. Note that all curves intersect at a common point A where C_{ℓ_I} = 0 when $\alpha_T = \alpha^*$.

The curves of ACG versus time in Fig. 13 are then interpreted in the following manner. With a ACG = 0.3 inch, for example, roll resonance will be maintained until point C_1 for Γ = -22.5 deg, because the magnitude of the ACG is greater than that of the corresponding curve. After point C_1, roll breakout will occur since a larger ACG than exists is required to maintain roll resonance. Between points C_2 and C_3 roll resonance would again occur if the roll rate were set equal to the pitch natural frequency. However, once breakout from roll resonance is achieved in the dynamic case, the roll rate rapidly approaches the nominal programming and the resulting trim angle of attack is greatly reduced. Other orientations of the asymmetries will yield breakout at different times (and angle of attack) as depicted by points C_4 and C_5. A ACG of 0.7 inch would yield roll lock-in for Γ = +22.5.

The choice of ACG tolerance is then made on the basis of the largest ACG yielding breakout from roll resonance for any orientation Γ. This means that the level of ACG under consideration must cross all curves of the parameter Γ at least once. For instance, in Fig. 13, it can be seen that all curves of Γ will intercept the line BE at least once, and that point B represents the highest value of ACG for which this will be the case, when C_{m_0} = 0.15.

From this latter consideration, it can be seen that a point where all curves intersect will then be at least a conservative value of ACG (e.g., point A when C_{ℓ_I} = 0 at $\alpha_T = \alpha_T^*$). With increasing levels of trim asymmetry (C_{m_0} or ε), this intersection point retrogresses in time and eventually yields the largest ACG tolerance.

When this intersection point yields zero ACG, the maximum trim asymmetry tolerance is defined. A similar set of curves is also found for thrust misalignment.

The same procedure can be used to determine the maximum allowable ACG for specified angle of attack at breakout from roll resonance. For example, in Fig. 13, the angle of attack reaches α_T = 2.0 deg at 41 sec. Point D then represents the largest allowable ACG for which breakout will occur before α_T exceeds 2.0 deg. For this case of small C_{m_0}, the ACG for angle of attack limitation is only slightly less than for roll lock-in.

Asymmetry Tolerance Contours

Evaluation of the ACG tolerance for an appropriate range of C_{m_0} and ϵ yields the asymmetry tolerance contours shown in Fig. 14 for the Aerobee 150A vehicle.

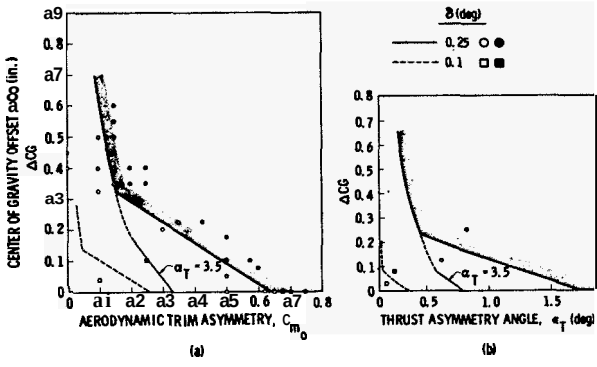

Fig. 14 Center of Gravity Tolerance Limits

These contours are interpreted as follows: asymmetry combinations below and to the left of the contour will not lock-in for any possible orientation within the body, although significant roll disturbance and angle of attack growth may occur prior to breakout. Above and to the right of the contour, there exists at least one orientation arrangement which will lock-in wherein roll resonance persists throughout the atmospheric portion of the flight. For the nominal fin cant of 0.25 deg, the aerodynamic asymmetry contour yields an intercept magnitude of C_{m_0} = 0.64 corresponding to a static trim angle of attack of 0.95 deg at sustainer burnout. The corresponding maximum thrust asymmetry of ϵ = 1.7 deg for 0 c.g. offset is far in excess of measurement capability of 0.1 deg. For smaller trim asymmetries, the allowable c.g. offset increases rapidly. For example, at C_{m_0} = 0.1, the ACG tolerance is a 0.6 inch lateral offset. At the nominal resonance time, this corresponds to an unbalance weight of 40 lb attached to one fin tip!

For the nominal fin cant angle of 0.25 deg, these contours exhibit quite reasonable asymmetry tolerances, particularly with respect to the thrust asymmetry. The aerodynamic trim asymmetry, although more difficult to assess, provides adequate ACG tolerance if care is exercised in configuration alignment and surface profile control. A requirement for limiting the angle of attack significantly reduces the longitudinal trim asymmetry tolerances, as indicated by the α_T = 3.5 deg contour. A drastic reduction of both ACG and C_{m_0} or ϵ occurs for a reduced fin cant of 0.1 deg as illustrated by the dashed contours. This arises primarily from the increase in resonant altitude with smaller fin cant. The larger resonant trim amplification occurring later in the flight decreases the allowable C_{m_0} or ϵ for a given ΔCG.

Verification of the Contours

These tolerance limits were tested with dynamic solutions for the time-varying environment. The testing of the operational criteria is summarized in Fig. 14 where each symbol spotted on the figure represents one or more dynamic solutions. Open symbols denote that roll lock-in did not occur for any arrangement of the asymmetries, although roll resonance may have been encountered for some period. Solid symbols depict cases for which roll lock-in occurred with subsequent catastrophic increase in angle of attack. For all of these cases, no restriction on maximum angle of attack nor roll rate recovery was imposed.

Note that some cases slightly above the maximum contour did not lock-in. This is attributed to the lag of the dynamic solution in reaching the equilibrium condition for which the tolerances were determined. This lag effect manifests itself in two ways – an increase in the phase shift, and a decrease in the maximum trim angle of attack at resonance. The estimated region of the dynamic lag effects is shown by the shaded areas above the contour. The agreement of the dynamic solutions with the equilibrium criteria appeared to be consistent for all C_{m_0}. Similar behavior and agreement between the dynamic solutions and equilibrium criteria was obtained for thrust asymmetry and with reduced fin cant of 0.1 deg.

The results of Fig. 14 demonstrate that the operational tolerance limits developed upon the basis of equilibrium trim response are verified quite satisfactorily. Furthermore, the dynamic solutions show that the equilibrium solutions yield conservative tolerances.

The assessment of roll lock-in for the purpose of verifying the tolerance limits is illustrated in Fig. 15 with ACG = 0.5 inch. Increasing C_{m_0} from 0.1 to 0.125 significantly increases the duration of roll resonance

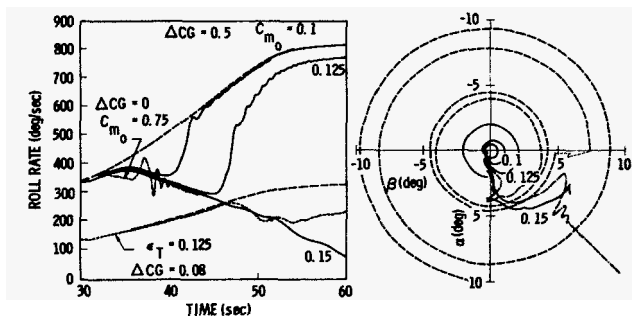

Fig. 15 Verification of Roll Lock-in Criteria

until lock-in is attained with C_{m_0} = 0.15. The angle of attack shows a gradual increase in trim magnitude until breakout occurs: this is followed by oscillations about a reduced trim. Where lock-in occurs, the angle of attack continues to grow in an orientation yielding a negative induced roll moment term. When the angle of attack is less than α^*, the α_T orientation exhibits a phase shift of only 45 deg. As α_T is approached and exceeded, additional phase shift accrues because the induced roll moment becomes positive. When the a~ rotates to the next region of negative induced roll, the orientation is stabilized and catastrophic growth of angle of attack proceeds.

The same general behavior of the angle of attack response occurs for high C_{m_0} = 0.75 (beyond the intercept) yielding roll lock-in with zero ACG. The gradual buildup of the trim along one fin shifts to the stable orientation midway between the fins as α_T exceeds α^*. In addition, roll oscillations about resonance induce large orientation oscillations.

The motion behavior for 0.1 deg fin cant exhibits similar characteristics as depicted for the thrust asymmetry case, where roll lock-in is observed until sustainer

thrust termination. The angle of attack grows in the prescribed manner during lock-in, with subsequent oscillations about trim after burnout. However, the amplitude of the oscillations continues to grow with time because the roll rate can no longer recover to the desired magnitude due to the reduced dynamic pressure. The spiral motion in the body-fixed axes represents simple coning in space, with a period of about 520 sec.

The motions exhibited in Fig. 15 for a fin cant of 0.1 deg clearly demonstrate the reduced motion control when resonance occurs late in the trajectory.

Comparison With Flight Behavior

A comparison of the roll lock-in motion behavior of Aerobee 150A Flight No. **4.04** with predicted roll lock-in response demonstrates striking similarities, as illustrated in Fig. 16. The motion data was extracted from Higgens[12] where a large precession coning motion was reported (prior to despin) withahalf cone angle of 89 deg.

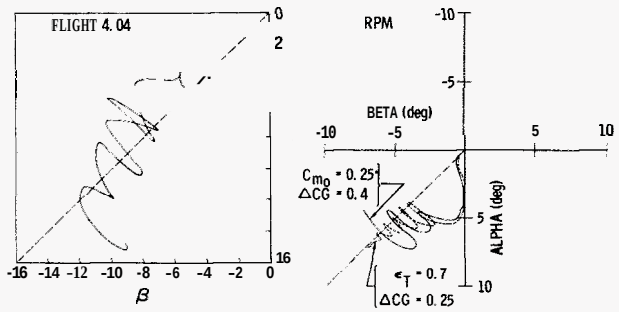

Fig. 16 Comparison With Flight Experience

Typical lock-in behavior was clearly evident in the roll history of Fig. 1A. Note in Fig. 16 that the roll rate is locked-in slightly above resonance, as borne out by the inside loop of the α-β motion, and the trim motion is clockwise. Initial roll resonance therefore occurred well above nominal resonance where the α_{TRIM} is small. Hence, substantial **ACG** must have been present. The asymmetry arrangement yielding this behavior is depicted on the simulation plot of α-β. The growth of angle of attack with an orientation slightly clockwise from the α axis arises from the induced roll moment being negative for $\alpha < \alpha^*$. When α^* is exceeded, the clockwise shift continues until the stable orientation midway between the fins is attained. The large oscillations in the orientation during catastrophic growth of the angle of attack are characteristic for large ΔCG and small trim asymmetry. Both simulations exhibit this behavior.

Comparison With Other Vehicles

The asymmetry tolerance contours of Fig. 14 were computed with constant linear aerodynamic characteristics except for the pitching moment (a function of time) and the induced roll moment (a function of the angle of attack). A coniparison of the normalized tolerance contours including variable aerodynamics is presented in Fig. 17 for the Aerobee 150A and *350* vehicles. A significant increase in the allowable asymmetries for the larger Aerobee *350* vehicle is clearly evident. The source is found in the relatively larger fin span for the Aerobee **350,** which **provides** a larger driving moment and increased α^*. The shadinq of the lee fins by the body requires a larger angle **of** attack to reverse the induced roll moment caused by the trailing nose vortices. This comparison serves to point out the importance of the fin characteristics to the roll lock-in asymmetry tolerances.

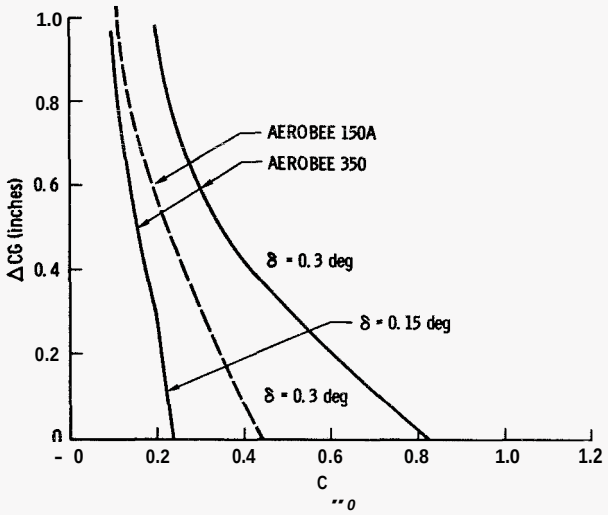

Fig. 17 Comparison of Aerodynamic Asymmetry Tolerances

IV. IN-FLIGHT ROLL CONTROL

The development of the understanding of the roll resonance phenomena described in the preceding sections naturally led to an investigation of means for positive control of the dynamic behavior during flight. Identification of the sources and establishment of the mechanisms leading to roll lock-in suggested several promising techniques for in-flight control of the motion. Three techniques for control of the roll rate were investigated: **(1)** Reaction Impulse. (2) Aerodynamic Surface Deflection, and *(3)* Center of Gravity Shift. The relative merits of these methods were evaluated upon the basis of simplicity, reliability. weight, size, and adaptability to operational and development vehicles. The efficacy of a given control technique was determined by the amount of improvement obtained in the preflight asymmetry tolerances.

Two methods are available for breaking out from roll resonance for combinations of asymmetry above the asymmetry tolerance: **(1)** overpower the asymmetry roll moment or (2) reduce the asymmetry roll moment directly. The former can be accomplished by an auxiliary roll moment to increase the roll driving moment from the fin cant. The latter can be accomplished by reducing the angle of attack or by appropriately displacing the c. g. The three techniques for in-flight roll control investigated represent different hardware approaches to these two methods, or combinations thereof.

The mechanism for accomplishing the roll rate increase or angle of attack reduction is illustrated in Fig. 18 in terms of the total rolling moment coefficient. The condition represented by the tolerance contours are reproduced here from Fig. 12 by the solid curves. If the asymmetry combination exceeds the tolerance contour, roll resonance occurs at point E_1 and will remain locked in throughout the entire flight (point E_2). Application of a rolling moment (A $\overline{}$ B) by means of a reaction moment (RM) or tip aileron deflection (δ_a) will increase the effective fin driving moment above the asymmetry moment and provide breakout to point F. With removal of the auxiliary roll moment at a later time (G → H), the solution will gravitate toward point F'. Since breakout will occur for the tangency condition, the applied moment can overcome a larger magnitude of either ΔCG or C_{m_0} and ϵ depicted by point E3.

In a similar manner, the application of a pitching moment or **a** lateral **c.g.** shift can reduce the magnitude of the asymmetry roll moment, as shown in Fig. 18b. The pitch moment reduces the angle of attack,

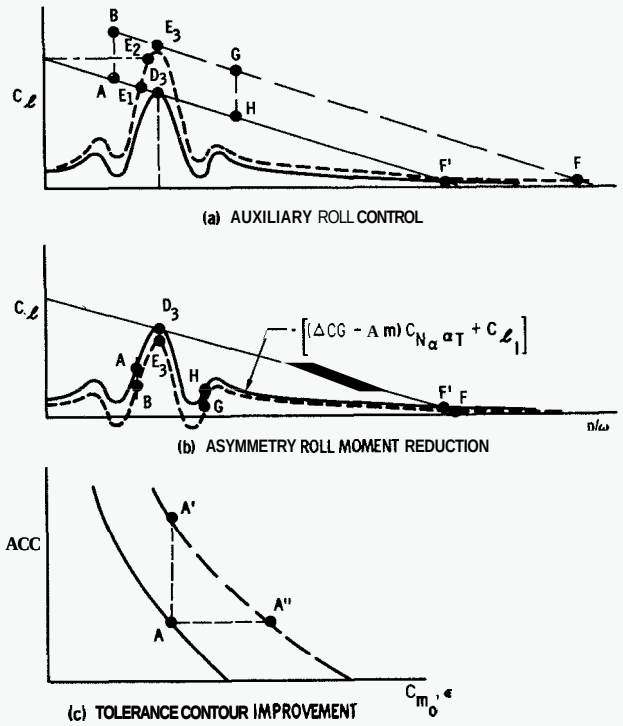

Fig. 18 Motion Control Methods and Tolerance Contour Improvement

thereby decreasing the magnitude of the normal force and the induced roll moment C_{ℓ_I}. The c.g. shift (Am) acts directly on the normal force coupling (ACG - Am). In either case, the nominal fin driving moment exceeds that caused by the asymmetries and drives the roll rate toward point F. When the auxiliary moments are released. the solution gravitates toward point F'. Again, the applied moments can overcome a larger asymmetry combination of ACG, C_{m_o} or ϵ equivalent to raising point E_3 to D_3.

This is exactly the procedure used to establish the tolerance contours of Fig. 14. Therefore, a new tolerance contour can be established by considering the aileron deflection, reaction moment, or c.g. shift to be acting throughout the entire trajectory, as depicted in Fig. 18c. A typical point on the original contour shifts from A to A' for a c.g. shift, reaction roll moment impulse or aileron deflection, and to A'' for a reaction pitch impulse or a pitch aerodynamic surface deflection. This solution technique can be applied equally well to the limit angle of attack contours or the roll lock-in contours. As a matter of fact, in the process of assessing the roll lock-in contours, the angle of attack contours are determined also.

The improvement of the Aerobee 350 roll lock-in tolerance contours for representative control moment magnitudes are summarized in Fig. 19 for aerodynamic trim asymmetry, with similar results for thrust asymmetry. Very significant increase in tolerable asymmetry levels to avoid roll lock-in is evident. For example, the 500 ft-lb roll reaction impulse increases the aerodynamic trim asymmetry intercept by 41 percent and the thrust asymmetry by 60 percent. These results suggest unlimited improvement with increasing control magnitudes. However, trajectory and vehicle characteristics limit the improvement for the intercept trim asymmetries. The value of the intercept depends only upon the time of resonant altitude (for $\delta = 0.3$ deg, t = 32 sec, so that C_{m_o} = 0.82 and ϵ = 1.53). Application of a roll moment yields a new resonance time (t= 29 sec for Rm = 500 ft/lb, for example) resulting in C_{m_o} = 1.17 and ϵ = 2.47 deg in Fig. 19. This procedure suggests that for sufficiently

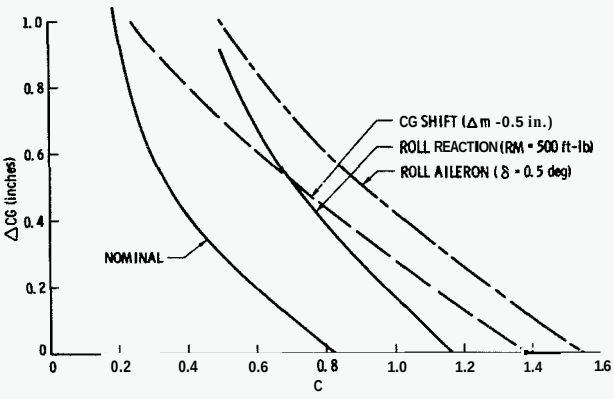

Fig. 19 Tolerance Contour Comparison – Aerodynamic Asymmetry (6 = 0.3 Deg)

large control magnitudes, it may be possihle to eliminate tolerances altogether. However, operational limits such as maximum roll rate within the atmosphere or maximum vacuum roll rate will restrict the usable increase. Careful consideration must also be given to the most appropriate initiation time for, and the duration of. the control application.

The contour improvements were verified with dynamic solutions via the RPM computer program utilizing the appropriate timing criteria. The results indicated a slightly reduced degree of conservatism for control application contours by comparison with the original contours.

Effect of Roll Rate Limitations

The duration of the control moment application for the improved tolerance contours of Fig. 19 were sufficient to handle a maximum of ACG of 1.0 inch. Reduction of the duration to minimize energy requirements (e.g., reaction impulse) or to satisfy an operational limit such as maximum roll rate can lead to a significant restriction of the usable improvement in the contours. The effects of a roll rate limitation upon the maximum contour improvement is illustrated in Fig. 20 for the tip aileron

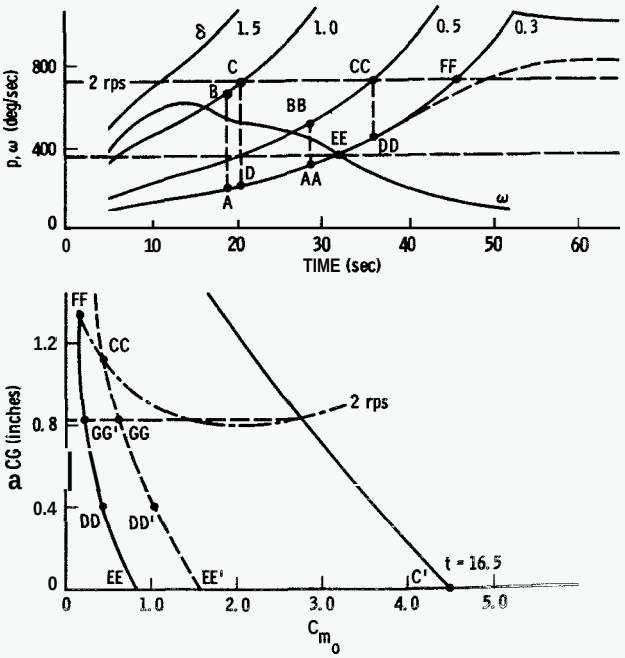

Fig. 20 Effect of Roll Rate Limit

roll control technique. The spin limit is based on the roll rate attained at termination of the roll control with no asymmetries acting.

By increasing the magnitude of the applied control to the equivalent of fin cant angle of **1.0** deg, a fourfold increase in the ΔCG-C_{m_0} tolerance contour can be achieved (point C'). The intercept magnitude of **4.47** corresponds to a new resonant time of **16.5** sec, indicated by the upper plot of equilibrium spin rate and aerodynamic pitch frequency. Utilizing a **1.5** deg fin cant would appear to yield an infinite intercept tolerance, since at booster burnout the roll rate is already above resonance. However, since the roll rate history in both cases parallels the aerodynamic pitch frequency, an extended period of resonance could occur for small differences in fin cant or pitch stability. Hence, fin cant angles up to **1.0** deg (or the equivalent for other techniques) probably represent a reasonable upper limit.

It is immediately apparent from Fig. **20** that imposition of a maximum roll rate limit **of 2** rps, for example, will constrain the usable improvement in the tolerance contour. Along the original contour for $\delta = 0.3$ deg, the intercept C_{m_0} of **0.83** occurs at **32.1** sec (point EE). The equilibrium roll rate reaches **2** rps at **45.8** sec (FF), which corresponds to ACG = **1.35** inches on the tolerance contour. Hence, the Aerobee **350** vehicle can accommodate a range of $C_{m_0} = 0.83$; ACG = 0 to $C_{m_0} = 0.15$; ACG = **1.35** inches with no control application under the constraint of a maximum roll rate of **2** rps. Application to other deflections yields the **2** rps spin rate boundary shown in Fig. **20.**

With a deflection from $\delta = 0.3$ deg to $\delta = 0.5$ deg. (point AA to BB), the limiting roll rate is reached at **36** sec (CC). Release of the control deflection to point DD corresponds to an allowable ACG of **0.4** inch on the original contour rather than **1.12** inches on the control contour for $\delta = 0.5$ deg. Since the angle of attack is equal to α^* along any of the contours, the ACG of point CC would cause roll resonance again. Hence, a ACG of **0.4** inch represents the maximum allowable along the control contour (point DD'). The asymmetry contour is then represented by EE' to DD' (on the $\delta = 0.5$ deg curve) to DD (at constant ACG) through FF (on the original contour). Thus, in order to accommodate a ACG of **0.83** inch, the control application of $\delta = 0.5$ deg must be maintained until **42** sec, which results in a maximum roll rate of **2.75** rps.

If the **2** rps constraint is applied to the fin cant of **1.0** deg, the value of control is completely negated. This is illustrated in Fig. **20** by the points labeled ABCD. After fin deflection from A to B, the roll rate attains **2** rps at C (**20.5** sec). Return to $\delta = 0.3$ deg (D) returns the roll rate to below resonance with subsequent roll lock-in after point EE, because the asymmetry combination is well above the original contour. In order to handle the ACG = **0.83** inch and $C_{m_0} = 2.75$ combination, the control application must again be maintained for **42** sec.

A number of mechanization schemes were evaluated including reaction impulse, aerodynamic fin tip glove, fin trailing edge spoiler, balance mass release, and fin tip ailerons. The most promising device proved to be the gyro-aileron illustrated in Fig. **21** capable of roll rate programming.

The mechanism consists of a spring-loaded tip aileron with a wind-driven-gyro actuator. The torsion spring preload deflects the aileron against the stop at **5** deg for the design shown. (The spring unloads at 8 deg deflection.) The gyro wheel spins at a rate proportional to velocity. The vehicle roll motion torques the **gyro** which precesses and deflects the aileron in the direction to reduce **roll** rate. The spring preload is set to equal the gyro precession torque at the desired spin rate, at which time the aileron just begins to come off the stop. The increasing wheel spin rate continues to reduce the aileron

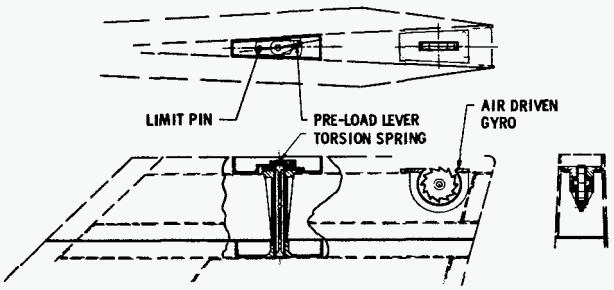

Fig. 21 Gyro Aileron

deflection throughout the flight, A limit pin can also be used to restrict negative deflections. The device applied to two fins is fairly light (**13** lb including a 1-lb damper). A 2-lb wheel with speeds up to 60,000 rpm appears satisfactory for nearly constant roll rate programming. No timer or power source is required if passage through resonance with the deflected aileron at an earlier time is satisfactory. A pin puller could be used to maintain zero aileron deflection until the desired initial time in order to reduce the angle of attack response. The additional weight would be about **1.1** lb for two fins.

The predicted steady roll rate performance **for** gyro spin rate proportional to velocity is illustrated in Fig. **22.** The spring preload condition is determined by the

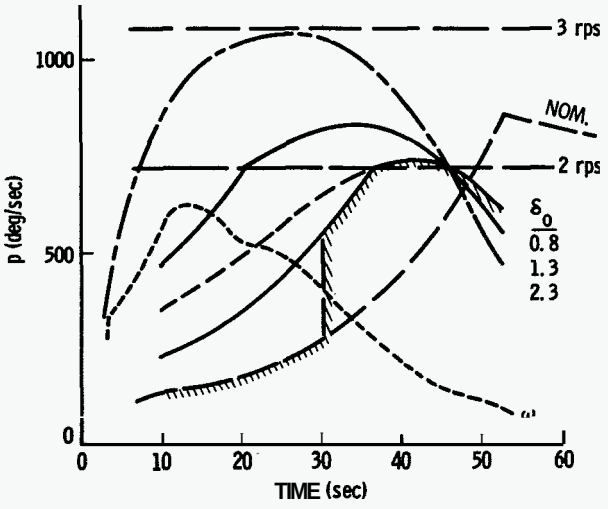

Fig. 22 Spin Rate Programming With Gyro Aileron

aileron deflection angle and the nominal spin rate required. For example, with a $\delta = 0.5$ and **2** rps, an unloaded aileron deflection of $\delta_0 = 0.8$ is required. The spin rate response without the deflection stop is shown by the dashed line up to **2** rps at **35.8** sec increasing to about **2.06** rps maximum and dropping below **2** rps after **45.5** sec. This second point is selected by the ACG tolerance to be accommodated (see Section II). With a deflection limit at $\delta = 0.5$ the roll response is depicted by the heavy curve for which resonance occurs at **26.5** sec. If the aileron is restrained at zero deflection until **30** sec, the roll rate response indicated by the hatched lines results. With a larger aileron deflection (e.g., $\delta = 1.0$), **2** rps roll rate is reached earlier at **20.5** sec, increasing to a maximum of **2.3** rps. Thus, very reasonable roll rate programs can be achieved even for large deflections. The roll rate responses of Fig. **22** suggests the use of the gyro-aileron to program roll rate above resonance immediately, such as depicted by the curve

for $\delta_o = 2.3$. This program represents essentially a continuation of the booster roll programming. Large aileron cant angles are required but the loads experienced are mild. For example, in order to yield 600 deg/sec roll rate in 5 sec, a constant aileron force of 13 lb is required for two fins.

The suggested roll program can accrue very large benefits in terms of the asymmetry tolerance improvement. Theoretically, the tolerances are infinite since the roll rate is always above resonance, and the rolling trim angle of attack is zero. In actual practice, however, normal fin cant deviations, etc., can yield roll rates closer to resonance, resulting in a rolling trim angle of attack other than zero with consequent roll coupling. But since the aerodynamic damping is large in this flight regime, angle of attack amplification at resonance is relatively small and roll resonance may not be especially objectionable. The asymmetry tolerances to breakout from resonance can be easily defined by methods of Section II. An additional feature of the roll programming by the gyro aileron is the reduction of roll rate late in the flight. While the flight vehicle cannot respond to the steady state roll rates depicted in Fig. 22 due to lag at high altitudes, reasonably low roll rates can be expected. This gyro aileron retains all of the advantages of the tip aileron (i.e., high roll effectiveness, low weight and simplicity), in addition to providing the advantages of roll programming.

REFERENCES

1. Nelson, R. L., "Measurement of Aerodynamic Characteristics of Reentry Configurations in Free Flight at Hypersonic and Near-Orbital Speeds," AGARD Report 380, Fluid Dynamics Panel Specialists Meeting on Use of Rocket Vehicles in Flight Research, Scheveningen, The Netherlands, July 1961.

2. Nelson, R. L., "The Motions of Rolling Symmetrical Missiles Referred to a Body-Axis System." NACA TN 3737, November 1956.

3. Nelson, R. L., and Niewald, R. J., "Some Effects of Steady Roll on the Dynamic Behavior of a Ballistic Reentry Test Vehicle," Transactions of The First Technical Symposium on Ballistic Missiles, WDD. ARDC, 21-22 June 1956.

4. Nelson, R. L., Louis, C. A., and Woods, P. S.. "Methods for Controlling the Angle of Attack of a Spinning Missile During Reentry," Proceedings of the Fourth U. S. Navy Symposium on Aeroballistics, Bureau of Ordnance, NAVORD Report No. 5904, 1 May 1958.

5. Smelt, R., "Lockheed X17 Rocket Test Vehicle and Its Applications," ARS Journal, Vol. 29, No. 7, July 1959.

6. Kanno, J. S., "Spin Induced Forced Resonant Behavior of a Ballistic Body Reentering the Atmosphere," LMSC 288139, Vol. 3, LMSD, Sunnyvale, California. January 1960.

7. Glover, L. S., "Analytical Expressions for the Effect on Roll Rate of Mass and Aerodynamic Asymmetries for Ballistic-Type Bodies," Johns Hopkins, APL-TG 560, March 1964.

8, Nicolaides, J. D., "Two Nonlinear Problems in the Flight Dynamics of Modern Ballistic Missiles," IAS Report No. 59-17, January 1959.

9. Mann, E. K., and McNemery, J. D., "Aerobee 150 Flight Dynamics Study," Space General Corporation Report No. 358, FR 1-11, January 1964.

10. Herbert, P. J., and Merchant, D. G., "The Importance of Pitch-Yaw Rolling Moments on the Motion of the Skylark Research Vehicles," RAE GW TN 583, July 1963.

11. Lawrence, J. T., "Aerobee 150A Aerodynamic Data from NOL Wind Tunnel Tests," GSFC Report X671-64-47, February 1964.

12. Higgens, L., "Rocket Performance and Telemetry Data Report, NASA 4.04 (Aerobee)," New Mexico University, PSL Report No. 4, 14 October 1960.